MRAC-Based Admittance Control for Aerial Physical Interaction

Ishaq Hafez* and Karl Stol
Department of Mechanical and Mechatronics Engineering, University of Auckland, Auckland 1010, New Zealand

ABSTRACT

This paper presents an admittance controller with model reference adaptive control (MRAC) for a fully actuated multirotor in physical interaction, in which an adaptive input drives the compliant response toward a reference compliance model. The admittance parameters are updated online through Lyapunov-based adaptation, while an MRAC position controller compensates matched translational uncertainty. Lyapunov analyses establish bounded tracking and parameter errors for the individual adaptive subsystems under the stated assumptions. Simulations on a fixed-tilt octocopter in single-point contact with a flexible cantilever beam show reduced interaction-axis tracking error and oscillations, increased beam-tip deformation, and greater robustness to parametric uncertainty than fixed admittance, with peak forces below the contact force limit.

1 INTRODUCTION

Aerial robots are increasingly employed in tasks requiring controlled physical interaction, including nondestructive inspection, infrastructure maintenance, and collaborative manipulation with humans [1, 2, 3]. Unlike fixed-base manipulators, unmanned aerial vehicles (UAVs) must regulate flight dynamics and contact forces simultaneously, which couples compliance, tracking accuracy, and contact safety. This creates a trade-off between compliance and precision: high compliance improves interaction safety but degrades free-flight tracking, whereas high stiffness improves positioning but can produce large impact forces and contact instability [4]. This trade-off motivates a control architecture that adapts compliant interaction and position tracking together under contact and model uncertainty.

Adaptive admittance control strategies have been developed for UAV physical interaction. Hamaza et al. [5] implemented an adaptive compliance mechanism on a quadrotor with a compliant arm by tuning torsional spring gains online to shape the force–position behavior during contact. For sustained contact in aerial manipulation, Marković et al. [6] used adaptive stiffness estimation within an impedance controller to regulate interaction with unknown environment stiffness. These approaches improve robustness to payload changes, unmodeled contact dynamics, and external disturbances, but adapt only the interaction layer. Simultaneous adaptation with motion tracking remains largely unexplored.

MRAC has addressed model uncertainty and external disturbances in UAV-manipulator systems. Orsag et al. used Lyapunov-based MRAC on a two-arm aerial manipulator to compensate center-of-mass and inertia variations, with a hybrid gain-scheduled extension [7, 8]. Sumathy and Ghose combined feedback linearization with MRAC to estimate uncertain parameters for a quadcopter with a 3-DoF arm [9]. Ali and Li developed an LQR-MRAC framework for a quadrotor with a 2-DoF gripper under payload-induced uncertainty [10]. Other studies address varying payloads and online estimation of mass, thrust, inertia, and center-of-gravity changes [11, 12]. These studies show reference-model adaptation compensates for payload changes, inertia shifts, and reaction forces, but does not adapt compliant behavior, such as force regulation, in coordination with trajectory tracking.

Aerial physical interaction requires simultaneous adaptation of compliant contact behavior and motion tracking under uncertainty. Prior works either employ an outer-loop MRAC with inner-loop controllers or use impedance or admittance control to shape interaction dynamics without MRAC position tracking, including adaptive stiffness and impedance control [6], interaction force and predictive admittance control on fully actuated platforms [1], port-Hamiltonian wrench and impedance regulation [13], and coordinated frameworks for compliant aerial manipulation [3]. Existing work does not combine MRAC-based input augmentation inside the admittance loop, Lyapunov-based admittance-parameter adaptation, and an MRAC position controller for adaptive aerial physical interaction. The proposed framework addresses this gap by adapting the contact response in the admittance layer and compensating matched translational uncertainty in the position loop. An MRAC term drives the admittance response toward a reference compliance model, while Lyapunov-based updates adapt the admittance parameters under contact and modeling variations.

Simulations evaluate the method on a fixed-tilt octocopter in contact with a flexible cantilever beam. A fixed-admittance baseline isolates the effect of online adaptation, while lateral and vertical contact-arm axes are considered to assess post-contact interaction-axis tracking error and oscillations under beam-model parametric uncertainty.

*Email address: ishaq.hafez@auckland.ac.nz

2 SYSTEM MODEL

The fixed-tilt octocopter (FT-X8) has eight rotors arranged in four fixed-tilt coaxial pairs [14], as shown in Fig. 1. This layout enables direct thrust along $\hat{\mathbf{x}}_b$ and $\hat{\mathbf{y}}_b$ without attitude changes and supports independent force and moment control. Contact is made through a body-mounted rigid contact arm whose axis is fixed in $\mathcal{F}_b$. The inertial frame $\mathcal{F}_n$ uses North-East-Down axes, and $\mathcal{F}_b$ is fixed at the center of mass with $\hat{\mathbf{z}}_b$ downward. Counter-rotating coaxial pairs cancel hover reaction torque, while differential thrust generates body-frame forces and moments. The attitude is parameterized by ZYX Euler angles $\boldsymbol{\eta} = [\phi, \theta, \psi]^\top$, where $\mathbf{R}_b^n$ maps $\mathcal{F}_b$ to $\mathcal{F}_n$ and $\mathbf{R}_n^b := (\mathbf{R}_b^n)^\top$. The body angular velocity $\boldsymbol{\omega}_b = [p,\ q,\ r]^\top$ satisfies $\dot{\boldsymbol{\eta}} = \mathbf{T}^{-1}(\phi, \theta)\boldsymbol{\omega}_b$ [12].

The translational dynamics in $\mathcal{F}_b$ are given by

$$m\big(\dot{\mathbf{v}}_b + \boldsymbol{\omega}_b \times \mathbf{v}_b\big) = mg\,\mathbf{R}_n^b \hat{\mathbf{z}}_n - \mathbf{C}_t\,\mathbf{v}_b + \mathbf{f}_b + \mathbf{f}_{e,b}, \quad (1)$$

where $m > 0$ is the mass, $\mathbf{v}_b := [\,v_{x,b}\ v_{y,b}\ v_{z,b}\,]^\top$ is the body-frame linear velocity, $g > 0$ is the gravitational acceleration, $\hat{\mathbf{z}}_n := [\,0\ 0\ 1\,]^\top$ is the inertial z-axis unit vector, $\mathbf{C}_t := \mathrm{diag}(C_{tx}, C_{ty}, C_{tz})$ is the translational drag matrix, $\mathbf{f}_b := [\,f_{x,b}\ f_{y,b}\ f_{z,b}\,]^\top$ is the total rotor thrust force, and $\mathbf{f}_{e,b} \in \mathbb{R}^3$ is the external contact force. Let $\mathbf{p}_n := [\,x_n\ y_n\ z_n\,]^\top$ denote the position in $\mathcal{F}_n$. Differentiating $\dot{\mathbf{p}}_n = \mathbf{R}_b^n\,\mathbf{v}_b$ and using (1) gives the inertial acceleration

$$\ddot{\mathbf{p}}_n = g\,\hat{\mathbf{z}}_n + \tfrac{1}{m}\,\mathbf{R}_b^n\big(\mathbf{f}_b - \mathbf{C}_t\,\mathbf{v}_b + \mathbf{f}_{e,b}\big). \quad (2)$$

The rotational dynamics in $\mathcal{F}_b$ are given by

$$\mathbf{J}\,\dot{\boldsymbol{\omega}}_b + \boldsymbol{\omega}_b \times (\mathbf{J}\,\boldsymbol{\omega}_b) = -\,\mathbf{C}_r\,\boldsymbol{\omega}_b + \mathbf{m}_b + \boldsymbol{\tau}_{e,b}. \quad (3)$$

where $\mathbf{J} := \mathrm{diag}(J_x, J_y, J_z)$ is the body inertia matrix, $\mathbf{C}_r := \mathrm{diag}(c_p, c_q, c_r)$ is the rotational damping matrix, $\mathbf{m}_b := [m_{x,b}\ m_{y,b}\ m_{z,b}]^\top$ is the rotor moment input, and $\boldsymbol{\tau}_{e,b} := [\tau_{e,x,b}\ \tau_{e,y,b}\ \tau_{e,z,b}]^\top$ is the external contact moment.

For rotor $i \in \{1, \ldots, 8\}$, let $\mathcal{F}_i$ be its local frame, $\hat{\mathbf{z}}_i$ its thrust axis, $\mathbf{R}_b^i$ the rotation from $\mathcal{F}_i$ to $\mathcal{F}_b$, and $\mathbf{p}_i := [x_i\ y_i\ z_i]^\top$ its position in $\mathcal{F}_b$. The total body wrench generated by the rotor thrusts and reaction torques is

$$\mathbf{w}_b := \begin{bmatrix} \mathbf{f}_b \\ \mathbf{m}_b \end{bmatrix} = \sum_{i=1}^{8} \begin{bmatrix} \mathbf{R}_b^i(f_i\,\hat{\mathbf{z}}_i) \\ \mathbf{R}_b^i(m_i\,\hat{\mathbf{z}}_i) + \mathbf{p}_i \times \mathbf{R}_b^i(f_i\,\hat{\mathbf{z}}_i) \end{bmatrix}. \quad (4)$$

The dynamics use $\mathbf{w}_b + \mathbf{w}_{e,b}$, where $\mathbf{w}_{e,b} := [\,\mathbf{f}_{e,b}^\top\ \boldsymbol{\tau}_{e,b}^\top\,]^\top$, with $\mathbf{f}_{e,b}$ and $\boldsymbol{\tau}_{e,b}$ entering (1) and (3), respectively. Each rotor follows $f_i = k_f \omega_i^2$ and $m_i = k_m \omega_i^2$ for $i \in \{1, \ldots, 8\}$, where ω_i is the rotor speed, and $k_f > 0$ and $k_m > 0$ are the thrust and drag torque coefficients. Coaxial rotor-wash effects are modeled approximately by assigning the lower rotors in each coaxial pair an effectiveness factor of 0.8. Collecting the FT-X8 rotor thrusts as $\mathbf{f}_r := [f_1\ \cdots\ f_8]^\top \in \mathbb{R}^8$ with fixed tilt angle β, (4) becomes $\mathbf{w}_b = \boldsymbol{\Lambda}\mathbf{f}_r$, where $\boldsymbol{\Lambda} \in \mathbb{R}^{6\times 8}$ is

$$\boldsymbol{\Lambda} = \begin{bmatrix} -s_\beta & -s_\beta & s_\beta & s_\beta & 0 & 0 & 0 & 0 \\ 0 & 0 & 0 & 0 & s_\beta & -s_\beta & -s_\beta & s_\beta \\ -c_\beta & -c_\beta & -c_\beta & -c_\beta & -c_\beta & -c_\beta & -c_\beta & -c_\beta \\ -\sigma_2 & \sigma_2 & \sigma_2 & -\sigma_2 & \sigma_1 & -\sigma_1 & -\sigma_1 & \sigma_1 \\ \sigma_1 & \sigma_1 & -\sigma_1 & -\sigma_1 & \sigma_2 & \sigma_2 & -\sigma_2 & -\sigma_2 \\ \sigma_3 & -\sigma_3 & \sigma_3 & -\sigma_3 & \sigma_3 & -\sigma_3 & \sigma_3 & -\sigma_3 \end{bmatrix},$$

where $c_\beta = \cos\beta$, $s_\beta = \sin\beta$, $\sigma_1 = \frac{\sqrt{2}}{4}D\cos\beta$, $\sigma_2 = \sigma_1 - \frac{k_m}{k_f}\sin\beta$, and $\sigma_3 = \frac{k_m}{k_f}\cos\beta + \frac{\sqrt{2}}{4}D\sin\beta$. Since $\mathrm{rank}(\boldsymbol{\Lambda}) = 6$ for $\beta \in (0, \frac{\pi}{2})$, the platform is fully actuated at the body-wrench level. Although the FT-X8 is overactuated, the controller design does not rely on rotor redundancy.

Let $\mathbf{u}_{b,\mathrm{cmd}} := [\,\mathbf{f}_{b,\mathrm{cmd}}^\top\ \mathbf{m}_{b,\mathrm{cmd}}^\top\,]^\top \in \mathbb{R}^6$ denote the commanded body wrench and $\mathbf{f}_{r,\mathrm{cmd}} := [\,f_{\mathrm{cmd},1}\ \cdots\ f_{\mathrm{cmd},8}\,]^\top \in \mathbb{R}^8$ the commanded rotor thrust vector. The allocator maps $\mathbf{u}_{b,\mathrm{cmd}}$ to feasible rotor thrusts using $\boldsymbol{\Lambda}$ and sets $\omega_{i,\mathrm{cmd}} = \sqrt{f_{\mathrm{cmd},i}/k_f}$. Motor dynamics are modeled as $\tau\dot{\omega}_i = \omega_{i,\mathrm{cmd}} - \omega_i$, where $\tau > 0$ is the motor time constant.

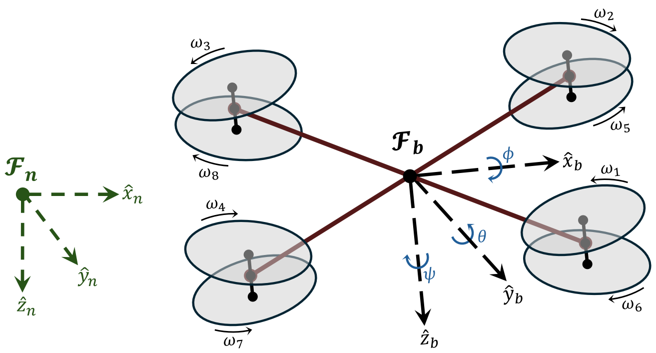

Figure 1: FT-X8 rotor layout with inertial and body frames.

3 CONTROL ARCHITECTURE

The control architecture in Fig. 2 maps the reference position and yaw command $\mathbf{r}_q(t) := [\,r_{x,n}(t)\ r_{y,n}(t)\ r_{z,n}(t)\ r_\psi(t)\,]^\top$ and the external wrench estimate $\hat{\mathbf{w}}_{e,n}(t) := [\,\hat{f}_{x,n}(t)\ \hat{f}_{y,n}(t)\ \hat{f}_{z,n}(t)\ \hat{m}_\psi(t)\,]^\top$ to compliant setpoints $\mathbf{q}_{sp}(t) := [\,x_{sp}(t)\ y_{sp}(t)\ z_{sp}(t)\ \psi_{sp}(t)\,]^\top$. The adaptive admittance layer regulates compliant interaction using an MRAC input and online parameter updates, while the MRAC position controller uses the translational components of $\mathbf{q}_{sp}(t)$ to generate $\boldsymbol{a}_{\mathrm{cmd}}(t) := [\,a_{x,n}(t)\ a_{y,n}(t)\ a_{z,n}(t)\,]^\top$ and compensate matched translational uncertainty. The inner flight controller and control allocation drive the plant to track $\boldsymbol{a}_{\mathrm{cmd}}(t)$ using cascaded attitude and rate PID loops [15].

3.1 Fixed Admittance Controller

The fixed admittance (FA) controller imposes a linear mass–spring–damper relation between wrench and compliant setpoint for $q \in \{x_n, y_n, z_n, \psi\}$. Let $r_{q,n}$, $q_{sp,n}$, and $\hat{f}_{q,n}$

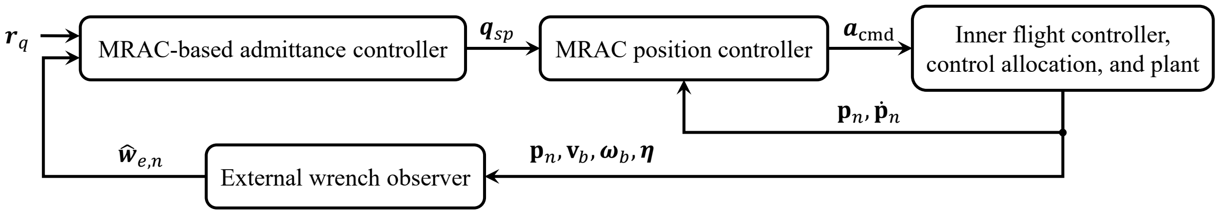

Figure 2: MRAC-based control architecture for aerial physical interaction.

denote the reference, compliant setpoint, and wrench component, and define $e_q^{\mathrm{c}}(t) := q_{sp,n}(t) - r_{q,n}(t)$. An observer [16] provides $\hat{\mathbf{w}}_{e,n}(t) \in \mathbb{R}^4$ from measured $(\mathbf{p}_n, \mathbf{v}_b, \boldsymbol{\omega}_b, \boldsymbol{\eta})$, while the plant is driven by the contact wrench $\mathbf{w}_{e,b}(t)$. The compliant setpoint follows a second-order admittance law [2].

$$M_q\big(\ddot{q}_{sp,n}(t) - \ddot{r}_{q,n}(t)\big) + C_q\big(\dot{q}_{sp,n}(t) - \dot{r}_{q,n}(t)\big) + K_q\big(q_{sp,n}(t) - r_{q,n}(t)\big) = \hat{f}_{q,n}(t). \tag{5}$$

with $M_q \in \mathbb{R}_{>0}$, $C_q \in \mathbb{R}_{>0}$, and $K_q \in \mathbb{R}_{>0}$. Equation (5) defines four decoupled second-order admittance filters on x_n, y_n, z_n, and ψ. Roll and pitch are stabilized by the inner loop and excluded from the admittance law.

3.2 *MRAC-Based Adaptive Admittance Control*

The FA law in (5) is sensitive to contact uncertainty, wrench estimation errors, unmodeled couplings, and fixed admittance parameters, which can cause residual offsets in $q_{sp,n} - r_{q,n}$. The proposed MRAC-based admittance uses $u_q(t)$ to drive $q_{sp,n}$ toward a reference model, while online parameter updates adapt the compliance dynamics. Introducing $u_q(t)$ gives the channel-q admittance dynamics

$$M_q\ddot{e}_q^{\mathrm{c}}(t) + C_q\dot{e}_q^{\mathrm{c}}(t) + K_q e_q^{\mathrm{c}}(t) = \hat{f}_{q,n}(t) + u_q(t). \tag{6}$$

Let $\mathbf{x}_q(t) := [\, q_{sp,n}(t) \;\; \dot{q}_{sp,n}(t)\,]^\top$. Equation (6) becomes

$$\dot{\mathbf{x}}_q(t) = \mathbf{A}_q\,\mathbf{x}_q(t) + \mathbf{B}_q\big(u_q(t) + \nu_q(t) + d_q\big),$$

$$\mathbf{A}_q := \begin{bmatrix} 0 & 1 \\ -\frac{K_q}{M_q} & -\frac{C_q}{M_q} \end{bmatrix}, \qquad \mathbf{B}_q := \begin{bmatrix} 0 \\ \frac{1}{M_q} \end{bmatrix},$$

where $d_q \in \mathbb{R}$ is an unknown constant matched disturbance representing wrench-estimation bias and unmodeled contact terms, and

$$\nu_q(t) := \hat{f}_{q,n}(t) + M_q\ddot{r}_{q,n}(t) + C_q\dot{r}_{q,n}(t) + K_q r_{q,n}(t)$$

is a known matched term. The desired reference model is

$$\dot{\mathbf{x}}_{\mathrm{ref},q}(t) = \mathbf{A}_{\mathrm{ref},q}\,\mathbf{x}_{\mathrm{ref},q}(t) + \mathbf{B}_{\mathrm{ref},q}\,r_{q,n}(t),$$

with $\mathbf{x}_{\mathrm{ref},q}(t) := [\, q_{\mathrm{ref},q}(t) \;\; \dot{q}_{\mathrm{ref},q}(t)\,]^\top$ and

$$\mathbf{A}_{\mathrm{ref},q} := \begin{bmatrix} 0 & 1 \\ -\omega_{n,q}^2 & -2\zeta_q\omega_{n,q} \end{bmatrix}, \quad \mathbf{B}_{\mathrm{ref},q} := \begin{bmatrix} 0 \\ \omega_{n,q}^2 \end{bmatrix},$$

where $\zeta_q > 0$ and $\omega_{n,q} > 0$, with settling time $T_{\mathrm{set},q} \approx 4/(\zeta_q\omega_{n,q})$. Define the admittance MRAC tracking error

$$\mathbf{e}_q^{\mathrm{m}}(t) := \mathbf{x}_q(t) - \mathbf{x}_{\mathrm{ref},q}(t) = \begin{bmatrix} q_{sp,n}(t) - q_{\mathrm{ref},q}(t) \\ \dot{q}_{sp,n}(t) - \dot{q}_{\mathrm{ref},q}(t) \end{bmatrix}.$$

The adaptive input is chosen in the direct MRAC form [17],

$$u_q(t) = \hat{K}_{q1}(t)\,q_{sp,n}(t) + \hat{K}_{q2}(t)\,\dot{q}_{sp,n}(t) + \hat{K}_{qr}(t)\,r_{q,n}(t) - \nu_q(t) - \hat{K}_{qd}(t),$$

where $\hat{K}_{q1}(t)$, $\hat{K}_{q2}(t)$, $\hat{K}_{qr}(t)$, and $\hat{K}_{qd}(t)$ are adaptive estimates. The term $-\nu_q(t)$ cancels the known matched term, and $\hat{K}_{qd}(t)$ compensates d_q. Assume ideal matching constants $K_{q1}^\star, K_{q2}^\star, K_{qr}^\star, K_{qd}^\star$ exist such that

$$\mathbf{A}_q + \mathbf{B}_q\begin{bmatrix} K_{q1}^\star & K_{q2}^\star \end{bmatrix} = \mathbf{A}_{\mathrm{ref},q}, \quad \mathbf{B}_q K_{qr}^\star = \mathbf{B}_{\mathrm{ref},q}, \quad K_{qd}^\star = d_q.$$

Define the parameter errors

$$\tilde{K}_{qi}(t) := \hat{K}_{qi}(t) - K_{qi}^\star, \qquad i \in \{1, 2, r, d\}.$$

Then the admittance MRAC error dynamics become

$$\dot{\mathbf{e}}_q^{\mathrm{m}}(t) = \mathbf{A}_{\mathrm{ref},q}\mathbf{e}_q^{\mathrm{m}}(t) + \mathbf{B}_q\Big(\tilde{K}_{q1}(t)q_{sp,n}(t) + \tilde{K}_{q2}(t)\dot{q}_{sp,n}(t) + \tilde{K}_{qr}(t)r_{q,n}(t) - \tilde{K}_{qd}(t)\Big). \tag{7}$$

Let $\mathbf{P}_q = \mathbf{P}_q^\top \succ 0$ solve

$$\mathbf{P}_q\mathbf{A}_{\mathrm{ref},q} + \mathbf{A}_{\mathrm{ref},q}^\top\mathbf{P}_q = -\mathbf{Q}_q, \qquad \mathbf{Q}_q = \mathbf{Q}_q^\top \succ 0,$$

and define $\sigma_q(t) := \mathbf{e}_q^{\mathrm{m}\top}(t)\mathbf{P}_q\mathbf{B}_q$. The adaptive laws are

$$\dot{\hat{K}}_{q1}(t) = -\Gamma_{q1}\,q_{sp,n}(t)\,\sigma_q(t),\; \dot{\hat{K}}_{q2}(t) = -\Gamma_{q2}\,\dot{q}_{sp,n}(t)\,\sigma_q(t),$$
$$\dot{\hat{K}}_{qr}(t) = -\Gamma_{qr}\,r_{q,n}(t)\,\sigma_q(t),\; \dot{\hat{K}}_{qd}(t) = \Gamma_{qd}\,\sigma_q(t),$$

with $\Gamma_{q1}, \Gamma_{q2}, \Gamma_{qr}, \Gamma_{qd} \in \mathbb{R}_{>0}$. For the Lyapunov function

$$V_q^{\mathrm{m}}(t) = \mathbf{e}_q^{\mathrm{m}\top}(t)\mathbf{P}_q\mathbf{e}_q^{\mathrm{m}}(t) + \frac{\tilde{K}_{q1}^2(t)}{\Gamma_{q1}} + \frac{\tilde{K}_{q2}^2(t)}{\Gamma_{q2}} + \frac{\tilde{K}_{qr}^2(t)}{\Gamma_{qr}} + \frac{\tilde{K}_{qd}^2(t)}{\Gamma_{qd}},$$

using (7) and the adaptive laws gives the derivative $\dot{V}_q^{\mathrm{m}}(t) = -\mathbf{e}_q^{\mathrm{m}\top}(t)\mathbf{Q}_q\mathbf{e}_q^{\mathrm{m}}(t) \le 0$. Thus, $\mathbf{e}_q^{\mathrm{m}}(t)$ and the parameter errors are bounded. Under standard MRAC conditions, $\mathbf{e}_q^{\mathrm{m}}(t) \to 0$.

The parameters (M_q, C_q, K_q) are updated online. Define

$$\hat{a}_{1,q}(t) := \frac{\hat{C}_q(t)}{\hat{M}_q(t)}, \quad \hat{a}_{0,q}(t) := \frac{\hat{K}_q(t)}{\hat{M}_q(t)}, \quad \hat{b}_q(t) := \frac{1}{\hat{M}_q(t)}.$$

Substituting into the admittance error dynamics (5) gives

$$\ddot{e}_q^{\mathrm{c}}(t) = -\hat{a}_{1,q}(t)\dot{e}_q^{\mathrm{c}}(t) - \hat{a}_{0,q}(t)e_q^{\mathrm{c}}(t) + \hat{b}_q(t)\hat{f}_{q,n}(t). \quad (8)$$

Let $\mathbf{x}_q^{\mathrm{c}}(t) := [\, e_q^{\mathrm{c}}(t) \;\; \dot{e}_q^{\mathrm{c}}(t)\,]^\top$ and define

$$\hat{\mathbf{A}}_q^{\mathrm{c}}(t) := \begin{bmatrix} 0 & 1 \\ -\hat{a}_{0,q}(t) & -\hat{a}_{1,q}(t) \end{bmatrix}, \qquad \mathbf{B}_c := \begin{bmatrix} 0 \\ 1 \end{bmatrix}.$$

Then the compliance error dynamics (8) becomes

$$\dot{\mathbf{x}}_q^{\mathrm{c}}(t) = \hat{\mathbf{A}}_q^{\mathrm{c}}(t)\,\mathbf{x}_q^{\mathrm{c}}(t) + \mathbf{B}_c\,\hat{b}_q(t)\hat{f}_{q,n}(t).$$

The ideal compliance model is specified by $a_{0,q}^\star = \omega_{n,q}^2$, $a_{1,q}^\star = 2\zeta_q\omega_{n,q}$, and $b_q^\star > 0$, with

$$\mathbf{A}_q^{\mathrm{c}\star} := \begin{bmatrix} 0 & 1 \\ -a_{0,q}^\star & -a_{1,q}^\star \end{bmatrix}.$$

Let $\mathbf{x}_{m,q}(t)$ be the state of the corresponding reference model

$$\dot{\mathbf{x}}_{m,q}(t) = \mathbf{A}_q^{\mathrm{c}\star}\,\mathbf{x}_{m,q}(t) + \mathbf{B}_c\,b_q^\star\hat{f}_{q,n}(t),$$

and define the compliance-model tracking error $\mathbf{e}_q^{\mathrm{cm}}(t) := \mathbf{x}_q^{\mathrm{c}}(t) - \mathbf{x}_{m,q}(t)$. The error dynamics are given by

$$\dot{\mathbf{e}}_q^{\mathrm{cm}}(t) = \mathbf{A}_q^{\mathrm{c}\star}\,\mathbf{e}_q^{\mathrm{cm}}(t) + \mathbf{B}_c\big(-\tilde{a}_{1,q}\dot{e}_q^{\mathrm{c}}(t) - \tilde{a}_{0,q}e_q^{\mathrm{c}}(t) + \tilde{b}_q\hat{f}_{q,n}(t)\big),$$

with $\tilde{a}_{1,q}(t) := \hat{a}_{1,q}(t) - a_{1,q}^\star$, $\tilde{a}_{0,q}(t) := \hat{a}_{0,q}(t) - a_{0,q}^\star$, and $\tilde{b}_q(t) := \hat{b}_q(t) - b_q^\star$. Let $\mathbf{P}_q^{\mathrm{c}} = \mathbf{P}_q^{\mathrm{c}\top} \succ 0$ solve

$$\mathbf{A}_q^{\mathrm{c}\star\top}\mathbf{P}_q^{\mathrm{c}} + \mathbf{P}_q^{\mathrm{c}}\mathbf{A}_q^{\mathrm{c}\star} = -\mathbf{Q}_q^{\mathrm{c}}, \qquad \mathbf{Q}_q^{\mathrm{c}} = \mathbf{Q}_q^{\mathrm{c}\top} \succ 0,$$

and define $\sigma_q^{\mathrm{c}}(t) := \mathbf{e}_q^{\mathrm{cm}\top}(t)\mathbf{P}_q^{\mathrm{c}}\mathbf{B}_c$. For $\Gamma_{a1,q}, \Gamma_{a0,q}, \Gamma_{b,q} \in \mathbb{R}_{>0}$, consider the Lyapunov function

$$V_q^{\mathrm{c}} = \mathbf{e}_q^{\mathrm{cm}\top}(t)\mathbf{P}_q^{\mathrm{c}}\mathbf{e}_q^{\mathrm{cm}}(t) + \frac{\tilde{a}_{1,q}^2}{\Gamma_{a1,q}} + \frac{\tilde{a}_{0,q}^2}{\Gamma_{a0,q}} + \frac{\tilde{b}_q^2}{\Gamma_{b,q}}.$$

Choosing

$$\begin{aligned} \dot{\hat{a}}_{1,q}(t) &= \Gamma_{a1,q}\,\dot{e}_q^{\mathrm{c}}(t)\,\sigma_q^{\mathrm{c}}(t), \\ \dot{\hat{a}}_{0,q}(t) &= \Gamma_{a0,q}\,e_q^{\mathrm{c}}(t)\,\sigma_q^{\mathrm{c}}(t), \\ \dot{\hat{b}}_q(t) &= -\Gamma_{b,q}\,\hat{f}_{q,n}(t)\,\sigma_q^{\mathrm{c}}(t), \end{aligned}$$

yields the derivative $\dot{V}_q^{\mathrm{c}}(t) = -\mathbf{e}_q^{\mathrm{cm}\top}(t)\mathbf{Q}_q^{\mathrm{c}}\mathbf{e}_q^{\mathrm{cm}}(t) \le 0$, so $\mathbf{e}_q^{\mathrm{cm}}(t)$, $\tilde{a}_{1,q}$, $\tilde{a}_{0,q}$, and $\tilde{b}_q$ are bounded and $\mathbf{e}_q^{\mathrm{cm}}(t) \to 0$ as $t \to \infty$. The adaptive admittance parameters are then

$$\hat{M}_q(t) = \frac{1}{\hat{b}_q(t)}, \;\; \hat{C}_q(t) = \frac{\hat{a}_{1,q}(t)}{\hat{b}_q(t)}, \;\; \hat{K}_q(t) = \frac{\hat{a}_{0,q}(t)}{\hat{b}_q(t)}.$$

The adaptive admittance for each channel is therefore

$$\hat{M}_q(t)\,\ddot{e}_q^{\mathrm{c}}(t) + \hat{C}_q(t)\,\dot{e}_q^{\mathrm{c}}(t) + \hat{K}_q(t)\,e_q^{\mathrm{c}}(t) = \hat{f}_{q,n}(t) + u_q(t),$$

where $u_q(t)$ drives $q_{sp,n}(t)$ toward the reference model, and $(\hat{M}_q, \hat{C}_q, \hat{K}_q)$ define the adaptive admittance dynamics.

3.3 *MRAC-Based Position Control*

The MRAC position controller tracks the translational components of $\mathbf{q}_{sp}(t)$ by commanding inertial accelerations on $q \in \{x_n, y_n, z_n\}$. From (2), with $\mathbf{x}_q(t) := [\, q_n(t) \;\; \dot{q}_n(t)\,]^\top$ and $u_q^{\mathrm{p}}(t) := a_{n,q,\mathrm{cmd}}(t)$, the matched-uncertainty model is

$$\dot{\mathbf{x}}_q(t) = \mathbf{A}\,\mathbf{x}_q(t) + \mathbf{B}\big(u_q^{\mathrm{p}}(t) + \mathbf{\Theta}_q^\top\mathbf{\Phi}_q(t) + d_q\big),$$

with

$$\mathbf{A} := \begin{bmatrix} 0 & 1 \\ 0 & 0 \end{bmatrix}, \qquad \mathbf{B} := \begin{bmatrix} 0 \\ 1 \end{bmatrix},$$

where $d_q \in \mathbb{R}$ is an unknown constant matched disturbance, $\mathbf{\Theta}_q \in \mathbb{R}^{p_q}$ is an unknown parameter vector, and $\mathbf{\Phi}_q(t) \in \mathbb{R}^{p_q}$ is a known regressor. The pair $(\mathbf{\Theta}_q, d_q)$ represents unmodeled acceleration terms. From (2), define $\boldsymbol{\rho}_q^\top(t) := \mathbf{i}_q^\top\mathbf{R}_b^n(t)$, where $\mathbf{i}_q$ is the unit vector along $q \in \{x_n, y_n, z_n\}$. Then

$$\mathbf{\Phi}_q(t) := \begin{bmatrix} \rho_{q1}(t)f_{x,b}(t) \\ \rho_{q2}(t)f_{y,b}(t) \\ \rho_{q3}(t)f_{z,b}(t) \end{bmatrix}, \qquad p_q = 3.$$

Choose a second-order reference model,

$$\dot{\mathbf{x}}_{\mathrm{ref},q}^{\mathrm{p}}(t) = \mathbf{A}_{\mathrm{ref},q}^{\mathrm{p}}\,\mathbf{x}_{\mathrm{ref},q}^{\mathrm{p}}(t) + \mathbf{B}_{\mathrm{ref},q}^{\mathrm{p}}\,q_{sp,n}(t),$$

where $\mathbf{x}_{\mathrm{ref},q}^{\mathrm{p}}(t) := [\, q_{\mathrm{ref},q}^{\mathrm{p}}(t) \;\; \dot{q}_{\mathrm{ref},q}^{\mathrm{p}}(t)\,]^\top$, and

$$\mathbf{A}_{\mathrm{ref},q}^{\mathrm{p}} := \begin{bmatrix} 0 & 1 \\ -\omega_{p,q}^2 & -2\zeta_{p,q}\omega_{p,q} \end{bmatrix}, \qquad \mathbf{B}_{\mathrm{ref},q}^{\mathrm{p}} := \begin{bmatrix} 0 \\ \omega_{p,q}^2 \end{bmatrix}.$$

The parameters $\omega_{p,q} > 0$ and $\zeta_{p,q} > 0$ tune the desired position transient. The position MRAC tracking error is

$$\mathbf{e}_q^{\mathrm{p}}(t) := \mathbf{x}_q(t) - \mathbf{x}_{\mathrm{ref},q}^{\mathrm{p}}(t) = \begin{bmatrix} q_n(t) - q_{\mathrm{ref},q}^{\mathrm{p}}(t) \\ \dot{q}_n(t) - \dot{q}_{\mathrm{ref},q}^{\mathrm{p}}(t) \end{bmatrix}.$$

The position control law on axis q is chosen as

$$\begin{aligned} u_q^{\mathrm{p}}(t) = \hat{K}_{x,q}^\top(t)\,\mathbf{x}_q(t) + \hat{K}_{r,q}(t)\,q_{sp,n}(t) \\ - \hat{\mathbf{\Theta}}_q^\top(t)\,\mathbf{\Phi}_q(t) - \hat{K}_{d,q}(t), \end{aligned}$$

with adaptive parameters $\hat{K}_{x,q}(t) \in \mathbb{R}^2$, $\hat{K}_{r,q}(t) \in \mathbb{R}$, $\hat{\mathbf{\Theta}}_q(t) \in \mathbb{R}^{p_q}$, and $\hat{K}_{d,q}(t) \in \mathbb{R}$. Assume ideal constants $K_{x,q}^\star \in \mathbb{R}^2$, $K_{r,q}^\star \in \mathbb{R}$, $\mathbf{\Theta}_q^\star \in \mathbb{R}^{p_q}$, and $K_{d,q}^\star \in \mathbb{R}$ such that

$$\begin{aligned} \mathbf{A} + \mathbf{B}K_{x,q}^{\star\top} = \mathbf{A}_{\mathrm{ref},q}^{\mathrm{p}}, &\quad \mathbf{B}K_{r,q}^\star = \mathbf{B}_{\mathrm{ref},q}^{\mathrm{p}}, \\ K_{d,q}^\star = d_q, &\quad \mathbf{\Theta}_q^\star = \mathbf{\Theta}_q. \end{aligned}$$

Define the position MRAC parameter errors

$$\tilde{K}_{x,q}(t) := \hat{K}_{x,q}(t) - K^{\star}_{x,q}, \quad \tilde{K}_{r,q}(t) := \hat{K}_{r,q}(t) - K^{\star}_{r,q},$$
$$\tilde{\boldsymbol{\Theta}}_q(t) := \hat{\boldsymbol{\Theta}}_q(t) - \boldsymbol{\Theta}^{\star}_q, \quad \tilde{K}_{d,q}(t) := \hat{K}_{d,q}(t) - K^{\star}_{d,q}.$$

Then the error dynamics for the position controller are

$$\dot{\mathbf{e}}^{\mathrm{p}}_q(t) = \mathbf{A}^{\mathrm{p}}_{\mathrm{ref},q}\,\mathbf{e}^{\mathrm{p}}_q(t) + \mathbf{B}\Big(\tilde{K}^{\top}_{x,q}(t)\,\mathbf{x}_q(t) + \tilde{K}_{r,q}(t)\,q_{sp,n}(t) - \tilde{\boldsymbol{\Theta}}^{\top}_q(t)\,\boldsymbol{\Phi}_q(t) - \tilde{K}_{d,q}(t)\Big).$$

Let $\mathbf{P}^{\mathrm{p}}_q = \mathbf{P}^{\mathrm{p}\top}_q \succ 0$ solve

$$\mathbf{P}^{\mathrm{p}}_q\mathbf{A}^{\mathrm{p}}_{\mathrm{ref},q} + \mathbf{A}^{\mathrm{p}\top}_{\mathrm{ref},q}\mathbf{P}^{\mathrm{p}}_q = -\mathbf{Q}^{\mathrm{p}}_q, \qquad \mathbf{Q}^{\mathrm{p}}_q = \mathbf{Q}^{\mathrm{p}\top}_q \succ 0.$$

Define $\sigma^{\mathrm{p}}_q(t) := \mathbf{e}^{\mathrm{p}\top}_q(t)\mathbf{P}^{\mathrm{p}}_q\mathbf{B}$. Use the Lyapunov function

$$V^{\mathrm{p}}_q(t) = \mathbf{e}^{\mathrm{p}\top}_q(t)\,\mathbf{P}^{\mathrm{p}}_q\,\mathbf{e}^{\mathrm{p}}_q(t) + \tilde{K}^{\top}_{x,q}(t)\,\boldsymbol{\Gamma}^{-1}_{x,q}\,\tilde{K}_{x,q}(t) + \frac{\tilde{K}^2_{r,q}(t)}{\Gamma_{r,q}} + \tilde{\boldsymbol{\Theta}}^{\top}_q(t)\,\boldsymbol{\Gamma}^{-1}_{\Theta,q}\,\tilde{\boldsymbol{\Theta}}_q(t) + \frac{\tilde{K}^2_{d,q}(t)}{\Gamma_{d,q}},$$

with $\boldsymbol{\Gamma}_{x,q}, \boldsymbol{\Gamma}_{\Theta,q} \succ 0$ and $\Gamma_{r,q}, \Gamma_{d,q} > 0$. Choosing

$$\dot{\hat{K}}_{x,q}(t) = -\boldsymbol{\Gamma}_{x,q}\,\mathbf{x}_q(t)\,\sigma^{\mathrm{p}}_q(t),$$
$$\dot{\hat{K}}_{r,q}(t) = -\Gamma_{r,q}\,q_{sp,n}(t)\,\sigma^{\mathrm{p}}_q(t),$$
$$\dot{\hat{\boldsymbol{\Theta}}}_q(t) = \boldsymbol{\Gamma}_{\Theta,q}\,\boldsymbol{\Phi}_q(t)\,\sigma^{\mathrm{p}}_q(t),$$
$$\dot{\hat{K}}_{d,q}(t) = \Gamma_{d,q}\,\sigma^{\mathrm{p}}_q(t),$$

yields the derivative $\dot{V}^{\mathrm{p}}_q(t) = -\mathbf{e}^{\mathrm{p}\top}_q(t)\mathbf{Q}^{\mathrm{p}}_q\mathbf{e}^{\mathrm{p}}_q(t) \le 0$. Therefore, $\mathbf{e}^{\mathrm{p}}_q(t)$ and the parameter errors are bounded. Under standard MRAC conditions, $\mathbf{e}^{\mathrm{p}}_q(t) \to 0$, provided the inner loop and allocation track within actuator limits.

4 RESULTS

The setup uses a body-mounted rigid contact arm whose tip contacts the free tip of a wall-mounted cantilever beam, as shown in Fig. 3. The beam acts as a compliant environment and generates an external wrench through the arm-tip reaction force. The beam centerline is aligned with $\hat{\mathbf{x}}_n := [1\ \ 0\ \ 0]^{\top}$ and has length $L_{\mathcal{B}}$. The UAV starts at $\mathbf{p}_n(0) = [0\ \ 0\ \ 0]^{\top}$ and tracks the undeformed beam-tip reference $\mathbf{p}_{T0,n} := [1\ \ 1\ \ -1]^{\top}$ over $T_{\mathrm{arr}} = 10$ s. The beam base is fixed at $\mathbf{p}_{0,n} := \mathbf{p}_{T0,n} - L_{\mathcal{B}}\,\hat{\mathbf{x}}_n$. This setup evaluates free-flight and contact operation without controller switching.

Let $\hat{\mathbf{a}}_b \in \mathbb{R}^3$ be the unit contact-arm axis fixed in $\mathcal{F}_b$, $s(t) \in [0, s_{\max}]$ the prescribed tip offset along this axis, and $\mathbf{r}_{a,b} \in \mathbb{R}^3$ the arm base. The arm-tip position and velocity are

$$\mathbf{r}_{c,b}(t) = \mathbf{r}_{a,b} + s(t)\,\hat{\mathbf{a}}_b, \qquad \dot{\mathbf{r}}_{c,b}(t) = \dot{s}(t)\,\hat{\mathbf{a}}_b.$$

The contact position and velocity in $\mathcal{F}_n$ are

$$\mathbf{p}_{c,n}(t) = \mathbf{p}_n(t) + \mathbf{R}^n_b(t)\,\mathbf{r}_{c,b}(t),$$
$$\mathbf{v}_{c,n}(t) = \dot{\mathbf{p}}_n(t) + \mathbf{R}^n_b(t)\big(\boldsymbol{\omega}_b(t) \times \mathbf{r}_{c,b}(t) + \dot{\mathbf{r}}_{c,b}(t)\big).$$

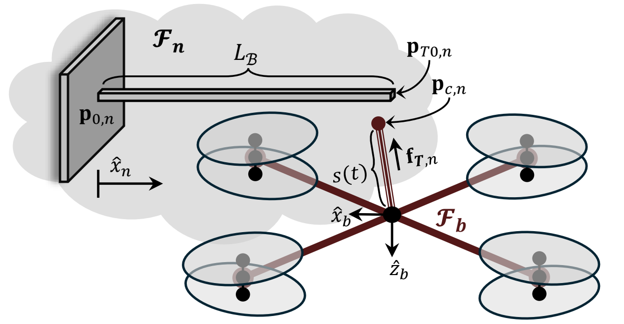

Figure 3: y_b-axis contact arm approaching a cantilever beam.

The beam-tip deformation in $\mathcal{F}_n$ is described by $\boldsymbol{\xi}(t) \in \mathbb{R}^3$,

$$\mathbf{p}_{T,n}(t) = \mathbf{p}_{T0,n} + \boldsymbol{\xi}(t), \qquad \mathbf{v}_{T,n}(t) = \dot{\boldsymbol{\xi}}(t).$$

The tip compliance is modeled by decoupled mass–spring–damper dynamics along the three inertial-frame axes:

$$\mathbf{M}_{\mathcal{B}}\,\ddot{\boldsymbol{\xi}}(t) + \mathbf{C}_{\mathcal{B}}\,\dot{\boldsymbol{\xi}}(t) + \mathbf{K}_{\mathcal{B}}\,\boldsymbol{\xi}(t) = \mathbf{f}_{T,n}(t),$$

where $\mathbf{M}_{\mathcal{B}}, \mathbf{C}_{\mathcal{B}}, \mathbf{K}_{\mathcal{B}} \in \mathbb{R}^{3\times 3}$ are mass, damping, and stiffness with $\mathbf{M}_{\mathcal{B}} \succ 0$, $\mathbf{C}_{\mathcal{B}} \succeq 0$, and $\mathbf{K}_{\mathcal{B}} \succeq 0$, and $\mathbf{f}_{T,n}(t) \in \mathbb{R}^3$ is the tip force in $\mathcal{F}_n$. Define the relative displacement and velocity between the arm tip and beam tip as

$$\mathbf{d}_p(t) := \mathbf{p}_{c,n}(t) - \mathbf{p}_{T,n}(t), \qquad \mathbf{d}_v(t) := \mathbf{v}_{c,n}(t) - \mathbf{v}_{T,n}(t).$$

Let $\hat{\mathbf{a}}_n(t) := \mathbf{R}^n_b(t)\hat{\mathbf{a}}_b$ denote the contact-arm axis in $\mathcal{F}_n$. Define the scalar contact penetration and penetration rate as

$$\delta(t) := \max\{0,\ \hat{\mathbf{a}}_n(t)^{\top}\mathbf{d}_p(t)\},\ \ \dot{\delta}(t) := \mathbb{I}_{\{\delta(t)>0\}}\,\hat{\mathbf{a}}_n(t)^{\top}\mathbf{d}_v(t).$$

Here $\mathbb{I}_{\{\delta(t)>0\}} = 1$ in contact and 0 otherwise. With contact stiffness $k_c > 0$ and damping $b_c \ge 0$, the contact force is

$$\mathbf{f}_{T,n}(t) := \max\{0,\ k_c\,\delta(t) + b_c\,\dot{\delta}(t)\}\,\hat{\mathbf{a}}_n(t). \tag{9}$$

The external wrench on the vehicle in $\mathcal{F}_b$ is

$$\mathbf{w}_{e,b}(t) := \begin{bmatrix} -\mathbf{R}^b_n(t)\,\mathbf{f}_{T,n}(t) \\ \mathbf{r}_{c,b}(t) \times \big(-\mathbf{R}^b_n(t)\,\mathbf{f}_{T,n}(t)\big) \end{bmatrix}.$$

The prescribed tip offset $s(t)$ ramps to $s_{\star}$, holds for T_{hold}, and ramps down symmetrically. The initial ramp is

$$s(t) = \frac{s_{\star}}{2}\left(1 - \cos\left(\pi\frac{t - T_1}{T_{\mathrm{ramp}}}\right)\right), \quad t \in [T_1,\ T_1 + T_{\mathrm{ramp}}].$$

In all simulations, $0 \le s(t) \le 0.02$ m, $s_{\star} = 0.02$ m, $T_1 = 10$ s, $T_{\mathrm{ramp}} = 3$ s, and $T_{\mathrm{hold}} = 20$ s. The contact wrench is applied only for $t \ge T_1$, with $\mathbf{w}_{e,b}(t) = \mathbf{0}$ for $t < T_1$. Let $T_c := [t^-_c,\ t^+_c]$ denote the contact interval, with $t^-_c \ge T_1$ and $|T_c| := t^+_c - t^-_c$. Two interaction cases are considered: y_b-axis and z_b-axis interaction with parametric uncertainty.

Simulations are performed in MATLAB R2024b with Simscape Multibody using the vehicle parameters in Table 1 and a single controller parameter set across all cases with $T_s = 1$ ms. For each $q \in \{x_n, y_n, z_n, \psi\}$, the admittance is second order with $M_q = 1$, $\zeta_q = 1$, $T^{c}_{set,q} = 2$ s, $\omega_{n,q} = 4/(\zeta_q T^{c}_{set,q})$, $K_q = M_q \omega^2_{n,q}$, and $C_q = 2\zeta_q M_q \omega_{n,q}$. The admittance reference model uses $T_{set,q} = 1.5\, T^{c}_{set,q}$ and $\zeta_q = 1$, with $\Gamma_{q1} = \Gamma_{q2} = \Gamma_{qr} = \Gamma_{qd} = 50$ and the adaptive admittance parameters initialized at the fixed-admittance values. The position MRAC reference model is critically damped with $T^{p}_{set} = 1$ s. The contact force limit $F_{max,c}$ is set to 60% of the available thrust margin above hover and is enforced by saturating the penetration at δ_{max} so that (9) does not exceed $F_{max,c}$. All beam and contact parameters are listed in Table 2.

Table 1: Vehicle and rotor model parameters.

Parameter	Value
Vehicle mass (m)	0.95 kg
Thrust coefficient (k_f)	1.21×10^{-6} N s^2/rad^2
Reaction torque coefficient (k_m)	1.04×10^{-8} N m s^2/rad^2
Motor time constant (τ)	0.15 s
Min rotor speed (ω_{min})	350 rad/s
Max rotor speed (ω_{max})	1774 rad/s
Rotor tilt angle (β)	31°
Arm length (l)	88.5 mm
Top rotor vertical offset (h_t)	35 mm
Bottom rotor vertical offset (h_b)	20 mm

Table 2: Beam and contact parameters.

Parameter	Value
Beam length ($L_{\mathcal{B}}$)	1 m
Tip mass ($\mathbf{M}_{\mathcal{B}}$)	diag(0.10, 0.02, 0.02) kg
Tip damping ($\mathbf{C}_{\mathcal{B}}$)	diag(204.74, 0.25, 0.25) N s/m
Tip stiffness ($\mathbf{K}_{\mathcal{B}}$)	diag(2.6×10^6, 10.78, 10.78) N/m
Contact force limit ($F_{max,c}$)	12 N
Penetration limit (δ_{max})	0.02 m
Contact stiffness (k_c)	600 N/m
Contact damping (b_c)	2.41 N s/m

4.1 *y_b-axis interaction with parametric uncertainty*

For the y_b case, $\hat{\mathbf{a}}_b = [0\ \ 1\ \ 0]^\top$ and $\hat{\mathbf{a}}_n(t) = \mathbf{R}^n_b(t)\hat{\mathbf{a}}_b$, as shown in Fig. 3. The UAV reaches $\mathbf{p}_{T0,n}$ by T_{arr}, after which $\mathbf{w}_{e,b}(t)$ is applied. Results compare FA with constant parameters against adaptive admittance (AA) with online updates and MRAC augmentation. Fig. 4 shows AA position tracking over the full task, while FA–AA differences are evaluated in the contact-response plots. Fig. 5 compares $\hat{\mathbf{a}}_n^\top \mathbf{p}_n$ and $\hat{\mathbf{a}}_n^\top \mathbf{q}_{sp,n}$. AA has smaller post-contact tracking error and reduced oscillations, indicating better interaction-axis tracking. Figs. 6 and 7 show greater beam-tip deformation during the prescribed arm motion, while the contact force remains below $F_{max,c}$.

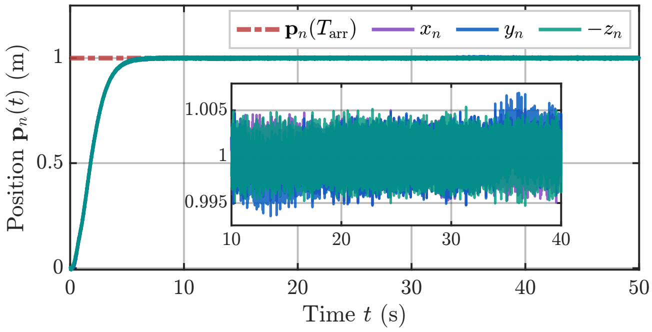

Figure 4: y_b-axis case: position components in $\mathcal{F}_n$.

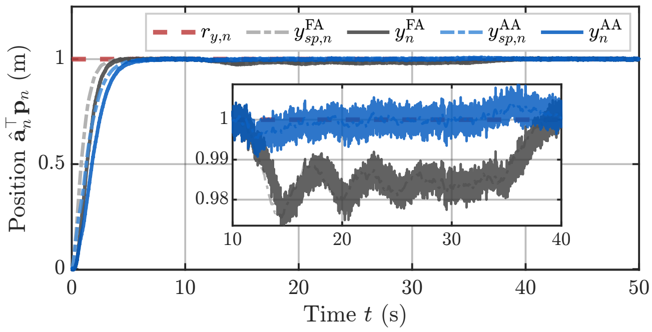

Figure 5: y_b-axis case: interaction-axis position and setpoint.

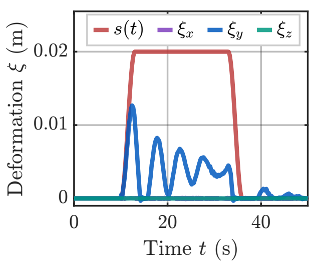

(a) Fixed Admittance.

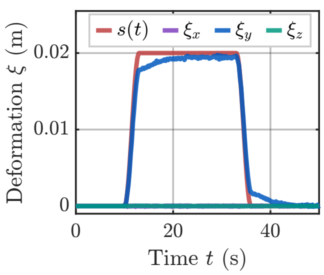

(b) Adaptive Admittance.

Figure 6: y_b-axis case: beam-tip deformation components.

For robustness, the beam matrices are scaled as $\mathbf{M}_{\mathcal{B}} \leftarrow \alpha\,\mathbf{M}_{\mathcal{B}}$, $\mathbf{C}_{\mathcal{B}} \leftarrow \alpha\,\mathbf{C}_{\mathcal{B}}$, and $\mathbf{K}_{\mathcal{B}} \leftarrow \alpha\,\mathbf{K}_{\mathcal{B}}$, with $\alpha \in \{0.25,\ 1.00,\ 1.25\}$. Over $T_c = [t_c^-, t_c^+]$, define $e_a(t) := \hat{\mathbf{a}}_n(t)^\top(\mathbf{p}_n(t) - \mathbf{q}_{sp,n}(t))$ and $\mathrm{MAE}_a := \frac{1}{|T_c|}\int_{t_c^-}^{t_c^+} |e_a(t)|\, dt$. The force metrics are $F_{\hat{\mathbf{a}},\max} := \max_{t \in T_c} \left|\hat{\mathbf{a}}_n(t)^\top \mathbf{f}_{T,n}(t)\right|$ and $F_{\hat{\mathbf{a}},\mathrm{MA}} := \frac{1}{|T_c|}\int_{t_c^-}^{t_c^+} \left|\hat{\mathbf{a}}_n(t)^\top \mathbf{f}_{T,n}(t)\right| dt$, and the deformation metric is $\xi_{\max} := \max_{t \in T_c} \left|\hat{\mathbf{a}}_n(t)^\top \boldsymbol{\xi}(t)\right|$. Table 3 shows that AA reduces MAE_a and increases $\xi_{\max}$ for all α.

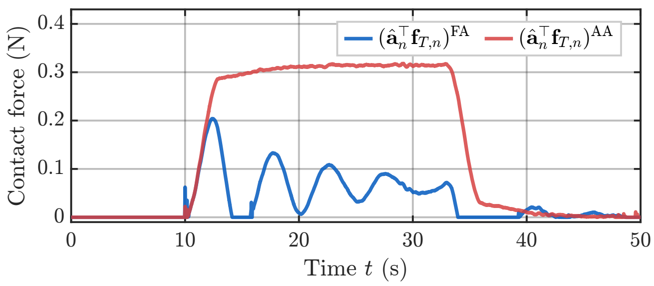

Figure 7: y_b-axis case: interaction-axis contact force.

Table 3: y_b-axis case: robustness under parameter scaling.

α	Metric	FA	AA
0.25	MAE_a (m)	6.46×10^{-4}	5.51×10^{-4}
	$F_{\hat{\mathbf{a}},\max}$ (N)	0.0718	0.0810
	$F_{\hat{\mathbf{a}},\mathrm{MA}}$ (N)	0.0267	0.0467
	$\xi_{\max}$ (m)	1.78×10^{-2}	2.01×10^{-2}
1.00	MAE_a (m)	1.50×10^{-3}	9.66×10^{-4}
	$F_{\hat{\mathbf{a}},\max}$ (N)	0.205	0.317
	$F_{\hat{\mathbf{a}},\mathrm{MA}}$ (N)	0.0449	0.183
	$\xi_{\max}$ (m)	1.27×10^{-2}	1.96×10^{-2}
1.25	MAE_a (m)	1.82×10^{-3}	1.13×10^{-3}
	$F_{\hat{\mathbf{a}},\max}$ (N)	0.237	0.394
	$F_{\hat{\mathbf{a}},\mathrm{MA}}$ (N)	0.0486	0.227
	$\xi_{\max}$ (m)	1.17×10^{-2}	1.95×10^{-2}

Greater deformation accompanies higher mean and peak contact forces, with $F_{\hat{\mathbf{a}},\max} \leq 0.394$ N $\ll F_{\max,c} = 12$ N.

4.2 *z_b-axis interaction with parametric uncertainty*

For the z_b case, $\hat{\mathbf{a}}_b = [0 \quad 0 \quad 1]^\top$, as shown in Fig. 8; FA and AA use the same contact profile. The AA full-task position response remains bounded and reaches the target, as in the y_b case. Figs. 9–11 show that AA reduces post-contact offset and oscillations and produces greater beam-tip deformation than FA under the same contact profile. The robustness study uses the same beam-parameter scaling as in Section 4.1, with $\alpha \in \{0.75, \ 1.00, \ 1.25\}$. Table 4 shows that AA reduces MAE_a and increases $\xi_{\max}$ for all α. Greater deformation accompanies higher mean and peak contact forces, with $F_{\hat{\mathbf{a}},\max} \leq 0.397$ N $\ll F_{\max,c} = 12$ N.

5 CONCLUSION

This paper presented an MRAC-based admittance architecture for aerial physical interaction. The admittance uses an MRAC input and Lyapunov-based parameter updates to follow a reference compliance model, while the MRAC position controller compensates matched translational uncertainty. The subsystem analyses establish bounded tracking and parameter errors under the stated assumptions. Simulations show reduced interaction-axis tracking error and greater beam-tip deformation relative to FA without exceeding the

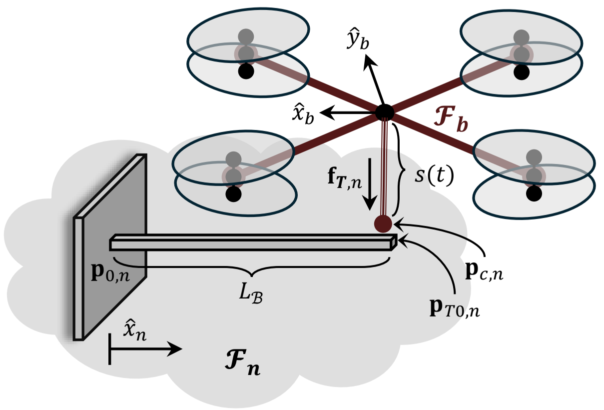

Figure 8: z_b-axis contact arm approaching a cantilever beam.

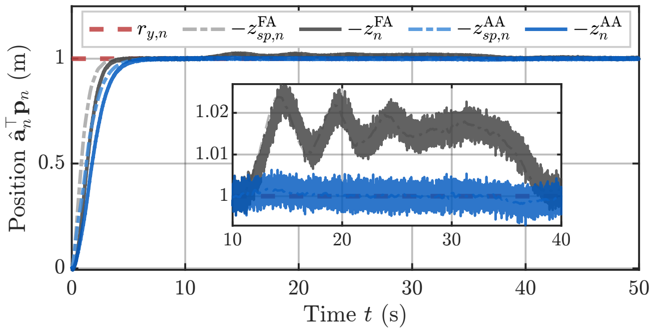

Figure 9: z_b-axis case: interaction-axis position and setpoint.

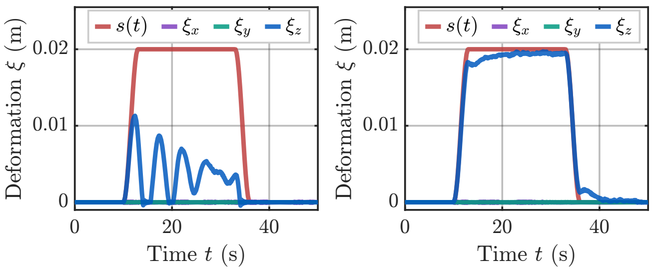

(a) Fixed Admittance. (b) Adaptive Admittance.

Figure 10: z_b-axis case: beam-tip deformation components.

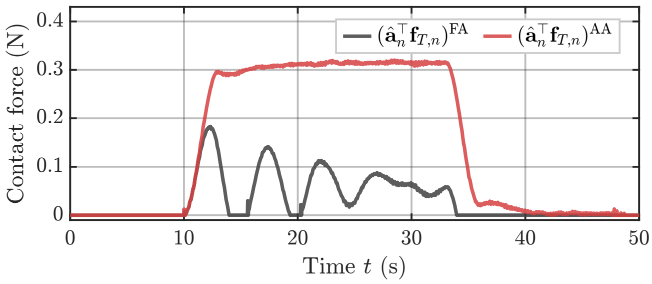

Figure 11: z_b-axis case: interaction-axis contact force.

Table 4: z_b-axis case: robustness under parameter scaling.

α	Metric	FA	AA
0.75	MAE_a (m)	1.26×10^{-3}	1.25×10^{-4}
	$F_{\hat{\mathbf{a}},\max}$ (N)	0.152	0.242
	$F_{\hat{\mathbf{a}},\mathrm{MA}}$ (N)	0.0596	0.142
	$\xi_{\max}$ (m)	1.25×10^{-2}	1.99×10^{-2}
1.00	MAE_a (m)	1.71×10^{-3}	1.34×10^{-4}
	$F_{\hat{\mathbf{a}},\max}$ (N)	0.184	0.322
	$F_{\hat{\mathbf{a}},\mathrm{MA}}$ (N)	0.0654	0.189
	$\xi_{\max}$ (m)	1.13×10^{-2}	1.97×10^{-2}
1.25	MAE_a (m)	2.29×10^{-3}	1.43×10^{-4}
	$F_{\hat{\mathbf{a}},\max}$ (N)	0.210	0.397
	$F_{\hat{\mathbf{a}},\mathrm{MA}}$ (N)	0.0697	0.233
	$\xi_{\max}$ (m)	1.04×10^{-2}	1.96×10^{-2}

contact force limit. Future work will extend the Lyapunov analysis to the coupled adaptive loops and validate the proposed architecture on the FT-X8 hardware.

ACKNOWLEDGEMENTS

The research was conducted as part of "Enabling Unmanned Aerial Vehicles (drones) to Use Tools in Complex Dynamic Environments UOCX2104", funded by the New Zealand Ministry of Business, Innovation and Employment.

REFERENCES

[1] K. Bodie, M. Brunner, M. Pantic, S. Walser, P. Pfändler, U. Angst, R. Siegwart, and J. Nieto. Active interaction force control for contact-based inspection with a fully actuated aerial vehicle. *IEEE Trans. Robot.*, 37(3):709–722, 2021.

[2] A. Alharbat, C. Gabellieri, A. Y. Mersha, and A. Franchi. Predictive admittance control for aerial physical interaction. *IEEE Robot. Autom. Lett.*, 10(11):11235–11242, 2025.

[3] M. Ryll, G. Muscio, F. Pierri, E. Cataldi, G. Antonelli, F. Caccavale, D. Bicego, and A. Franchi. 6D interaction control with aerial robots: The flying end-effector paradigm. *Int. J. Robot. Res.*, 38(9):1045–1062, 2019.

[4] H. N. Naser, H. A. Hashim, and M. Ahmadi. Human physical interaction based on UAV cooperative payload transportation system using adaptive backstepping and FNTSMC. In *Proc. Amer. Control Conf. (ACC)*, pages 450–456, 2025.

[5] S. Hamaza, I. Georgilas, and T. Richardson. Towards an adaptive-compliance aerial manipulator for contact-based interaction. In *Proc. IEEE/RSJ Int. Conf. Intell. Robots Syst.*, pages 7448–7453, 2018.

[6] L. Marković, M. Car, M. Orsag, and S. Bogdan. Adaptive stiffness estimation impedance control for achieving sustained contact in aerial manipulation. In *Proc. IEEE Int. Conf. Robot. Autom.*, pages 117–123, 2021.

[7] M. Orsag, C. Korpela, S. Bogdan, and P. Oh. Lyapunov based model reference adaptive control for aerial manipulation. In *Proc. Int. Conf. Unmanned Aircraft Syst.*, pages 966–973, 2013.

[8] M. Orsag, C. M. Korpela, S. Bogdan, and P. Y. Oh. Hybrid adaptive control for aerial manipulation. *J. Intell. Robot. Syst.*, 73(1):693–707, 2014.

[9] V. Sumathy and D. Ghose. Adaptive augmented torque control of a quadcopter with an aerial manipulator. *Drone Syst. Appl.*, 10(1):26–50, 2022.

[10] Z. A. Li and X. Li. Modeling and controlling of quadrotor aerial vehicle equipped with a gripper. *Measurement and Control*, 52(5-6):577–587, 2019.

[11] G. Baraban, M. Sheckells, S. Kim, and M. Kobilarov. Adaptive parameter estimation for aerial manipulation. In *Proc. Amer. Control Conf.*, pages 614–619, 2020.

[12] T. Maki, M. Zhao, F. Shi, K. Okada, and M. Inaba. Model reference adaptive control of multirotor for missions with dynamic change of payloads during flight. In *Proc. IEEE Int. Conf. Robot. Autom.*, pages 7433–7439, 2020.

[13] R. Rashad, J. B. C. Engelen, and S. Stramigioli. Energy tank-based wrench/impedance control of a fully actuated hexarotor: A geometric port-hamiltonian approach. In *Proc. IEEE Int. Conf. Robot. Autom.*, pages 6418–6424, 2019.

[14] P. H. M. Souza and K. Stol. Constrained dynamics of an aerial manipulator interacting with flexible cantilever beams. *IEEE/ASME Trans. Mechatronics*, 28(2):967–975, 2023.

[15] L. Meier, D. Honegger, and M. Pollefeys. PX4: A node-based multithreaded open source robotics framework for deeply embedded platforms. In *Proc. IEEE Int. Conf. Robot. Autom.*, pages 6235–6240, 2015.

[16] T. Tomić, C. Ott, and S. Haddadin. External wrench estimation, collision detection, and reflex reaction for flying robots. *IEEE Trans. Robot.*, 33(6):1467–1482, 2017.

[17] P. A. Ioannou and J. Sun. *Robust Adaptive Control*. Dover, Mineola, NY, 2012.